Int. J. Heat Mass Transfer. Vol. 28, No. 8, pp. 1487–1498
Printed in Great Britain

0017–9310/85 $3.00 + 0.00
Pergamon Press Ltd.

Theoretical and experimental study of transient and steady-state natural convection heat transfer from a vertical flat plate partially immersed in water

U. PROJAHN and H. BEER

Institut für Technische Thermodynamik, Technische Hochschule Darmstadt, Petersenstrasse 30, 6100 Darmstadt, F.R.G.

(*Received* 19 *October* 1984)

Abstract—Transient and steady-state heat transfer by natural convection from a vertical flat plate has been investigated both numerically and by experiment. The plate, loaded with a uniform and constant heat flux is positioned in a square container partially filled with liquid and gas. Solutions have been obtained for one set of thermophysical property ratios and for modified Rayleigh numbers up to $Ra^{*-} = 10^8$. This range has also been covered by experiments. Good agreement between calculated and measured results is obtained.

1. INTRODUCTION

HEAT TRANSFER in systems containing two or more immiscible components is not only of practical interest to a wide range of technologies but also for numerous natural processes.

The area of technical applications encompasses the wide field of vaporization and condensation processes as well as nuclear safety analysis, casting technology and metallurgical engineering. In the Hall process for aluminium smelting, for example, cryolite (Na_3AlF_6) and molten aluminium are stratified. In the presence of electromagnetic forces convective heat transfer will be affected additionally.

Direct-contact heat exchangers or the influence of air pockets on heat transfer in heat exchanger equipments are other applications of technical interest.

Heat transport in saturated fluids, where liquid and vapor phases of a single component fluid are stratified, often occur in technical systems. The safety of tanks containing liquified gases and exposed to external heat sources is of importance.

Further applications may be found in crystal growth processes where heat and mass transport are influenced additionally by thermo-capillary convection induced by surface tension effects, which lead to complex and sometimes oscillatory flows.

Although heat transport phenomena in two-phase systems are very important, investigations concerning the determination of free convection in multiple fluid layers are scarce. Szekely and Todd [1] studied, both numerically and experimentally, natural convection heat transfer in a rectangular box (height > width) filled with two unmixable high Prandtl number fluids. Cellular convection in a thin fluid layer (propylen-glycol/silicon-oil) heated from below was the object of a theoretical and experimental investigation performed by Stork [2]. He observed shearflow at the interface due to either kinematic decoupling at the interface as a result of contaminations or thermal effects. Heat transfer mechanisms due to natural convection in a rectangular box (width > height) containing two immiscible fluids with internal heat sources in the heavier one were studied by Schramm and Reineke [3] numerically and by experiment.

Bourde and Simanovskii [4] estimated stability characteristics for a system of two immiscible fluids heated from below by means of a finite-element analysis. The same configuration was treated by Simanovskii [5] using a finite-difference method for the solution of the conservation equations in stream-function–vorticity formulation. Numerical simulation of steady-state free convection heat transfer across a two-dimensional rectangular enclosure (height/width = 2) containing half and half air and water was the aim of Knight and Palmer [6]. Unfortunately the dimensionless governing equations based on streamfunction and vorticity are in error, which leads to valueless results.

The objective of the present study is the numerical and experimental investigation of transient and steady-state heat transfer from a vertical flat plate whose surface dissipates a uniform and constant heat flux and which is positioned in the middle of a square cavity containing two dissimilar fluids.

2. MATHEMATICAL FORMULATION

Considering general problems of convective heat transfer in two-phase systems it is obvious that the shape of the solution domain may be rather complex due to geometric form of enclosure and interface, which is often strongly curved and under some circumstances also time dependent. Therefore the code developed should be independent from the geometric contour as far as possible. This demand can be easily satisfied by applying numerically-generated body-fitted and in

NOMENCLATURE

a	thermal diffusivity
$\mathscr{A}, \mathscr{B}, \mathscr{C}$	general tensorial quantities
Bo	Bond number, equation (15)
D^{ij}	deformation tensor, $\frac{1}{2}d^{ij}$
$\mathscr{D}$	dilatation term
g	determinant of metric tensor
$\boldsymbol{g}_i$	covariant basis vector
$\sqrt{g}$	Jacobian of transformation
$\hat{g}$	acceleration of gravity
g_{ij}, g^{ij}	co- and contravariant components of the metric tensor
$\mathbf{G}$	gravity vector
h	film heat transfer coefficient
k	thermal conductivity
l	depth of immersion
L	length of plate
L_0	characteristic length, l
Ma^*	modified Marangoni number, $(\mathrm{d}\sigma/\mathrm{d}T)q''L_0^2/a\mu k$
n	coordinate in normal direction
Nu	Nusselt number, hL_0/k
p	pressure
Pr	Prandtl number, ν/a
q''	heat flux density
Ra^*	modified Rayleigh number, $\hat{g}\beta q''L_0^4/\nu ak$
s	coordinate
t	time
T	temperature
w^i	contravariant velocity component, $(w^1, w^2) \equiv (u, v)$
x^i	Cartesian coordinates $(x^1, x^2) \equiv (x, y)$.

Greek symbols

β	thermal expansion coefficient
ε	constants, equation (24)
ζ	equation (22), $f(Pr^{-1})$
ξ^i	curvilinear coordinate system, $(\xi^1, \xi^2) \equiv (\xi, \eta)$
μ	dynamic viscosity
ν	kinematic viscosity
ρ	density
σ	surface tension
ϕ	thermophysical property ratio.

Subscripts

i	derivative with respect to ξ^i
0	reference state
max	maximum
w	wall.

Superscripts

$+$	refers to the lighter fluid
$-$	refers to the heavier fluid
$\bar{}$	mean value.

general curvilinear coordinate systems. The grid generation method proposed by Thompson *et al.* [7] is used, where the coordinate systems are solutions of a system of quasi-linear partial differential equations of elliptic type. Compared with other transformation techniques, which are often valid only for a single class of geometric shapes, the proposed method has the great advantage that many geometric configurations of different kind can be treated with the computer program developed but once. Due to the experiences acquired during previous studies of various heat transfer problems (see e.g. [8–10]) the application of the proposed mapping technique proved to be a versatile tool in handling complex geometries and is therefore recommended for the elimination of the geometry as complicating factor.

2.1. *Conservation equations*

Employing general coordinates the equations conserving mass, momentum and energy have to be formulated generally for the continuous phases as well as for the interface phase. Starting with the integral form of the general conservation law (e.g. [11]) one obtains after some manipulations the following differential expressions for the conservation law

$$\left.\begin{aligned}(\partial/\partial t)\mathscr{A}^i\boldsymbol{g}_i + \frac{1}{\sqrt{g}}(\sqrt{g}\mathscr{A}^i\boldsymbol{g}_i w^j)_{,j} \\ + \frac{1}{\sqrt{g}}(\sqrt{g}\mathscr{B}^{ij}\boldsymbol{g}_i)_{,j} \\ + \mathscr{C}^i\boldsymbol{g}_i\end{aligned}\right\} = 0 \qquad (1)$$

where the tensor notation was employed as used for example in [12]. In equation (1) $\mathscr{A}$ is the quantity to be preserved, $\mathscr{C}$ is a source term and $\mathscr{B}$ represents the diffusive flux. The quantities $\mathscr{A}$ and $\mathscr{C}$ have the same tensorial order [vectors in (1)], while if $\mathscr{B} \neq 0$ then it is a one-order higher tensor [second-order tensor in (1)] than $\mathscr{A}$ or $\mathscr{C}$.

For the problem under study the resulting set of equations may be simplified by introducing the following assumptions:

- —The fluids are considered as Newtonian and incompressible.
- —All thermophysical properties are constant except for the density in the buoyancy term, where the Boussinesq approximation is adopted.
- —Validity of Fourier's law for isotropic media.

—Viscous dissipation is neglected.
—The fluid motion is regarded to be laminar and two-dimensional.

Regarding the restrictions given above, the general tensor components $\mathscr{A}$, $\mathscr{B}$, $\mathscr{C}$ which have to be substituted in (1) to get the conservation equations of mass, momentum and energy, reduce to:

mass:

$$\mathscr{A} = 1; \quad \mathscr{B}, \mathscr{C} = 0 \tag{2}$$

momentum:

$$\mathscr{A}^i = w^i; \quad \mathscr{B}^{ij} = (pg^{ij} - \mu d^{ij})/\rho; \quad \mathscr{C}^i = \beta(T - T_0)G^i \tag{3}$$

energy:

$$\mathscr{A} = T; \quad \mathscr{B}^i = -ag^{ij}T_{,i}; \quad \mathscr{C} = 0. \tag{4}$$

In view of the problem to be considered the following dimensionless variables are defined:

$$(x^i)^* = x^i/L_0; \quad (w^i)^* = w^i L_0/a^-;$$
$$p^* = pL_0^2/(\rho a^2)^-; \quad t^* = ta^-/L_0^2; \tag{5}$$
$$T^* = (T - T_0)k^-/(q'' L_0).$$

It should be noted that the choice of the reference quantities must be done carefully if a system of two immiscible fluids is considered. In the scope of the present study the thermophysical properties of the heavier fluid, denoted by a minus sign have been chosen for reference. Because the boundary condition of constant heat flux is prescribed at the heat emitting wall, the surface temperature is locally different and *a priori* unknown so that a characteristic temperature difference cannot be specified. For this reason it is convenient to use the relation $(q'' L_0)/k$ as reference quantity.

Substituting the quantities (5) into equation (1), the following non-dimensional set of governing equations results (the asterisks, denoting dimensionless quantities, are omitted for simplification):

continuity equation:

$$(\sqrt{g}w^i)_{,i} = 0 \tag{6}$$

momentum equations:

$$\left[(\partial/\partial t)w^i + \frac{1}{\sqrt{g}}(\sqrt{g}w^i w^j)|_j + \phi_1 g^{ij} p_{,j} + \phi_2 \frac{Pr^-}{\sqrt{g}}(\sqrt{g}d^{ij})|_j + \phi_3 \, \mathrm{Ra}^{*-} Pr^- G^i\right] g_i = 0 \tag{7}$$

where

$$d^{ij} = 2D^{ij} = w^j|_k g^{ki} + w^i|_k g^{kj}$$

energy equation:

$$(\partial/\partial t)T + \frac{1}{\sqrt{g}}(\sqrt{g}w^i T)_{,i} - \frac{\phi_4}{\sqrt{g}}(\sqrt{g}g^{ij}T_{,j})_{,i} = 0 \tag{8}$$

(a comma denotes partial differentiation, whereas | represents the covariant derivative).

The quantities ϕ_1–ϕ_4 are equal to one for the description of the heavier fluid (−) and contain ratios of thermophysical properties for consideration of the ligher phase (+). In detail:

$$\phi_1^+ = \rho^-/\rho^+; \quad \phi_2^+ = v^+/v^-;$$
$$\phi_3^+ = \beta^+/\beta^-; \quad \phi_4^+ = a^+/a^-. \tag{9}$$

2.2. *Interfacial boundary conditions*

For a complete description of the fluid system boundary conditions, which will be given later, coupling conditions at the fluid interface have to be specified. Performing an analogous analysis as described above, by considering the interface phase as a thin shell embedded in the three-dimensional Euclidian space and having particular material properties, general equations result which couple both adjacent phases. Details of this procedure, together with a more involved analysis of the derivation of the conservation equations, may be found in [13]. Restricting the mathematical model to a singular interface which undergoes no deformation due to fluid motion (an assumption which seems reasonable for the relatively low velocities occurring in natural convection processes) the following dimensionless set of equations, written for a coordinate line $\xi^2 = \text{const.}$ results in

no slip:

$$(w^1)^+ = (w^1)^- \tag{10}$$

no penetration:

$$(w^2)^+ = (w^2)^- = 0. \tag{11}$$

Momentum conservation,

tangential component:

$$\phi_5 A^+ - A^- + Ma^{*-} T_{,1}/\sqrt{g_{11}} = 0 \tag{12a}$$

normal component:

$$B^+ - B^- + Nb_1^1 = 0 \tag{12b}$$

where

$$A^{\pm} = \left[\sqrt{g}\left(d^{21} - \frac{g_{12}}{g_{11}}d^{22}\right)\right]^{\pm} \tag{12c}$$

$$B^{\pm} = \left[p + \phi_5 \, Pr^- \frac{g}{\sqrt{g_{11}}} d^{22}\right]^{\pm} \tag{12d}$$

$$\phi_5 = (\mu^+/\mu^-) \tag{12e}$$

$$N = \sigma L_0/(\rho a^2)^- \tag{12f}$$

continuity of temperature:

$$T^+ = T^- \tag{13}$$

continuity of heat flux:

$$\phi_6 C^+ - C^- = 0 \tag{14}$$

where

$$C^{\pm} = \left[\frac{1}{\sqrt{g}}\left(T_{,2} - \frac{g_{12}}{g_{11}} T_{,1}\right)\right]^{\pm} \tag{14a}$$

$$\phi_6 = (k^+/k^-). \tag{14b}$$

Examination of conditions (10)–(14) and the governing equations (6)–(8) reveals one extraneous interfacial boundary condition (12b). This is due to the *a priori* assumption of the interface location. In reality, the condition of momentum conservation in normal direction (12b), which is a generalization of the well-known Young–Laplace formula, serves for the determination of the exact shape of the interface. Presupposing an interface contour independent of fluid motion the location of the interface corresponds to that of the static fluid system and may be calculated by solving the Young–Laplace equation. A horizontal interface results, if the contact angle between interface and solid boundary is equal to $\pi/2$. For angles other than $\pi/2$ the assumption of a plane interface is justified if the Bond number, defined by

$$Bo = \hat{g}(\rho^- - \rho^+)L_0^2/\sigma \tag{15}$$

is very large ($Bo \gg 1$). Under terrestrial conditions this demand may be satisfied for fixed dimension L_0 if $\rho^- \gg \rho^+$, e.g. air and water.

2.3. *Pressure equation*

When considering compressible flows the density may be regarded as a dependent variable of the continuity equation. The pressure is then extracted via an equation of state. This approach is, however, inapplicable to incompressible fluids, where the density is independent of pressure changes. Therefore, the pressure distribution has to be determined in such a way, that the velocity components resulting from the momentum equations satisfy the continuity equation identically. Applying the divergence operator on equation (7) the desired equation, an elliptic PDE of Poisson type, for the direct calculation of pressure p is obtained as:

$$\frac{1}{\sqrt{g}}(\sqrt{g}g^{ij}p_{,j})_{,i} = \frac{1}{\sqrt{g}}\left[f(w^i)\right]_{,i} - (\partial/\partial t)\mathscr{D} \tag{16}$$

$\mathscr{D} = (1/\sqrt{g})(\sqrt{g}w^i)_{,i}$ is the so called dilatation term, which must be zero for the following time level $t = t + \Delta t$ to fulfill the continuity equation in the whole solution domain.

Projection of the vectorial equation (7) in the direction of the normal vector of boundary $\xi_i = \text{const.}$ leads to the corresponding boundary conditions of (16) which are all of Neumann type.

$$\left(\frac{g^{ij}}{\sqrt{g^{(ii)}}}p_{,j}\right) = \bar{f}(w^i) \quad \text{for} \quad \xi^i = \text{const.} \tag{17}$$

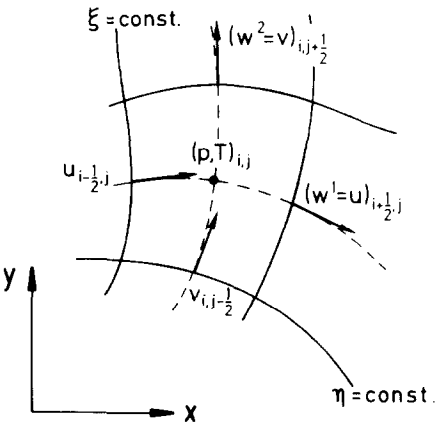

FIG. 1. Location of the dependent variables in the physical plane.

3. NUMERICAL PROCEDURE

The conservation equations given in terms of velocity and pressure (primitive variables) were solved by applying the finite-difference method. With regard to accuracy problems in primitive variable formulation, the question of variables location on the grid covering the solution domain is of special interest. To avoid oscillations in velocity or pressure fields an MAC-like arrangement of the variables is recommended [14], i.e. vectorial quantities (velocity) are located on the cell boundaries, while scalar quantities (pressure, temperature) are cell centered. Moving to curvilinear quadrilateral cells (Fig. 1) the special features of the MAC scheme are maintained if contravariant velocity components as used in the equations given above are employed.

The governing equations, (6)–(8), together with the Poisson equation for pressure (16), are discretized using only second-order central difference approximations in space and first-order backward differences in time. The resulting set of algebraic equations is solved by the Strongly Implicit Procedure (SIP) [15]. To avoid instability effects which may be introduced by the convective terms, the deferred correction method is applied. As pointed out the calculation of the pressure field requires the solution of a Poisson–Neumann problem. Because the coefficient matrix associated with equation (16) is singular (and has also lost the property of diagonal dominance in the case of general curvilinear coordinate systems), the numerical solution is difficult to find if methods like SIP, ADI, SOR, etc. are used. Therefore, an efficient algorithm based on the multigrid method was developed [16]. The proposed procedure permits a fast solution of equation (16) with a convergence rate independent of the number of equations.

4. PROBLEM UNDER CONSIDERATION

A schematic diagram of the problem under study, which should be regarded as a first step treating more

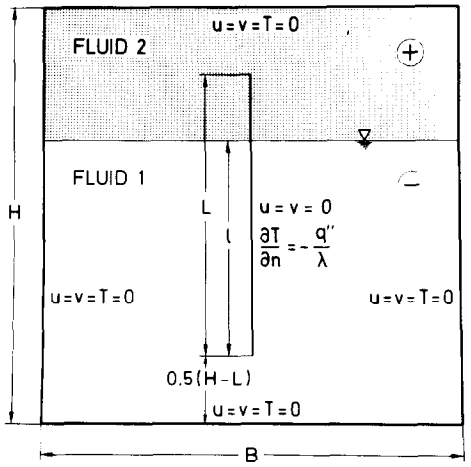

FIG. 2. Schematic representation of the problem under consideration with boundary conditions.

complex geometries, is depicted in Fig. 2. It shows a square container ($H = B$) partially filled with water (−) and bounded by isothermal walls. The remaining volume contains air (+). A vertical flat plate, loaded by a uniform and constant heat flux density q'', is fixed centrally. The plate has an overall length L and is immersed into the water by the distance l, which is also used as characteristic length L_0 ($l = L_0$).

At the rigid walls and at the heating surface no-slip conditions ($w^i = 0$) are used. The interfacial boundary conditions given above, but neglecting thermocapillary effects, are applied at the air–water interface. The limits of validity for neglecting Marangoni convection may be estimated by comparing modified Rayleigh and Marangoni numbers. For the fluid combination air/water thermal expansion coefficient and surface tension gradient ($d\sigma/dT$) have approximately the same order of magnitude. Therefore Ra^* and Ma^* depend essentially on the fourth and second power of the characteristic length, respectively, i.e. convection heat transfer will be influenced considerably only for small characteristic dimensions. For the dimensions used, thermal convection dominates which justifies the applied assumption.

5. APPARATUS AND EXPERIMENTAL PROCEDURE

The phenomena simulated numerically are verified by experimental investigations using the method of holographic interferometry. This optical method is well suited because complete information on the temperature field from the beginning to the steady-state condition is obtained. The test apparatus consists of a prismatic tank with a cross section of 120 × 120 mm. For visual observations two quartz glass windows 120 mm in diameter are placed in the centerline of the laser beam.

The main requirement for the heated vertical plate is a negligible heat capacity so that it can follow time-wise temperature variations readily. For this purpose a 0.05-mm-thick constantan foil is used. The advantages are a high specific and nearly temperature independent resistance. The foil (25 mm horizontally and 70 mm vertically) is fastened at a mounting support via isolated copper wires and is stretched tightly by four helical springs. Plate and mounting support can be twisted independently in order to allow an optimal alignment in the direction of the laser beam.

The ambient temperature within the water was monitored by a thermocouple mounted near the vertical plate and connected to a multi-channel recorder. After adjustment of the vertical foil, demineralized and carefully degassed water was poured into the test chamber to the desired depth of immersion. The entire system was then allowed to equilibrate.

A 50 mW He–Ne laser was used for holographic interferometry. Preceding the test a reference hologram under isothermal conditions has to be produced. During the tests, the object beam and the reference beam are superimposed. Changes in the fluid temperature and consequently changes in the refractive index are evidenced as interference patterns. All tests were performed using the adjustment of an infinite fringe field, i.e. the interference lines of a two-dimensional temperature field are interpreted as isotherms.

The test run starts with a step power input. For synchronization, the moment of closing the electric circuit is marked on the recorder. A 35-mm stills camera equipped with a motor drive is used to record the fast-changing interferograms. To assign the corresponding time to each photograph the marking device of the multichannel recorder was activated via the camera's flash contact. The foil heating current was measured during the test runs in order to determine the total power input and hence the heat flux density on the surface.

The local temperatures on the vertical plate were obtained from the interferograms. The evaluation procedure follows that given in [17] and is explained in [13], where further details of test section, test procedure and data reduction may be found.

To verify the test procedure heat transfer from a fully-submerged plate was studied first. A comparison with the theoretical results obtained by Sparrow and Gregg [18] showed very good agreement.

6. RESULTS AND DISCUSSION

As mentioned previously the investigation was performed for a system containing water and air. For the numerical calculations the following thermophysical properties [equations (9), (12e) and (14b)] based on a reference temperature of 20°C are used:

$$\phi_1 = 849.6; \quad \phi_2 = 16.8; \quad \phi_3 = 18.5;$$
$$\phi_4 = 152.2; \quad \phi_5 = 0.0198; \quad \phi_6 = 0.043; \quad (18)$$
$$Pr^+ = 0.7; \quad Pr^- = 7.0.$$

The heat transport was studied for three different depths of immersion, viz. $l/L = 0.25$, 0.5 and 0.75. The modified Rayleigh number based on the depth of immersion was varied in the range of $10^4 \leqslant Ra^{*-} \leqslant 10^8$. Referring to the dimensions realized in the experiment these Rayleigh numbers correspond to heat flux densities between 0.06 and 4700 W m^{-2}. The experiments were performed for $0.18 \leqslant l/L \leqslant 0.73$ and $489 \leqslant q'' \leqslant 906$ W m^{-2}, therefore covering Rayleigh numbers Ra^{*-} from 3.5×10^5 up to 1.4×10^8.

For the system depicted in Fig. 2 it is justified to regard the fluid motion around the vertical plate as symmetrical, which reduces the computational effort considerably. As a compromise between accuracy and costs a grid system totalling (50×25) and (70×33) nodal points was used for transient and steady-state calculations, respectively. For resolution of the steep gradients occurring at rigid boundaries at the interface and near the stagnation points, the grid lines are clustered there. Furthermore, the 'double grid approach' proposed by Pope [19] was used to get more accurate values of the metric coefficients.

6.1. *Transient heat transfer*

Since the first investigations by Illingworth [20] transient heat transfer from a vertical flat plate located in an infinite surrounding has been studied under various aspects. A review of these investigations may be found, for example in [21]. In contrast to the theoretical studies performed so far on this subject the full set of conservation equations has to be solved because the simpler boundary-layer equations are not applicable due to recirculating flow.

The timewise development of streamlines and temperature field, obtained by numerical simulation, is illustrated in Fig. 3 for some selected times and $Ra^{*-} = 2.8 \times 10^7$ $(l/L = 0.5)$. Isotherms and streamlines are depicted on the right- and left-hand side of each picture, respectively. The interface, separating the regions of water and air, appears as horizontal line. Immediately after loading the surface with a constant heat flux, heat is transferred solely by conduction. This leads to a temperature field parallel to the plate. Because of a uniform heat flux and due to the physical properties of the air, that portion of the surface exposed to the gas is heated to much higher temperatures, than the part in water. Therefore, convective motion develops much faster in the air layer and, as a consequence, the transient process is also shorter than in the liquid phase. This behavior is visualized by Fig. 3.

The circulation flow that already exists in the air-filled space for a short time after heating starts, induces a fluid motion in the water opposite to the flow generated by bouyancy forces. With increasing time, however, convective motion in the water is enhanced leading to a displacement of the secondary flow. Owing to the deflection of the fluid flow at the interface the isotherms spread fanwise and propagate along the interface.

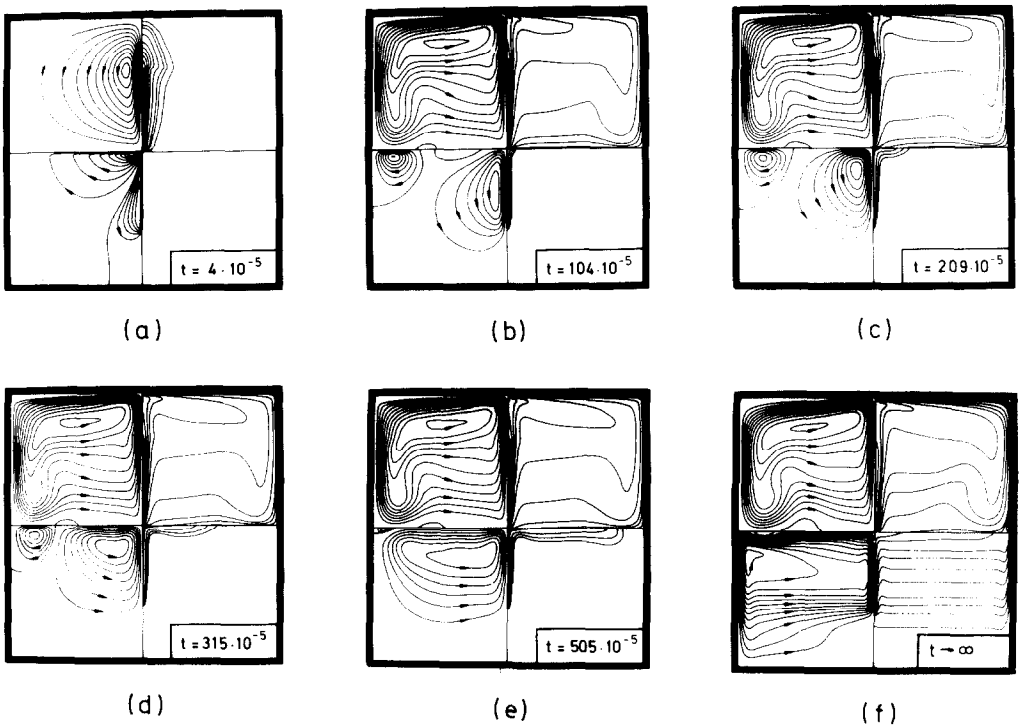

FIG. 3. Flow pattern (left) and temperature distribution (right) at different dimensionless times for $Ra^{*-} = 2.8 \times 10^7$ and $l/L = 0.5$ $(Pr^+ = 0.7, Pr^- = 7.0)$.

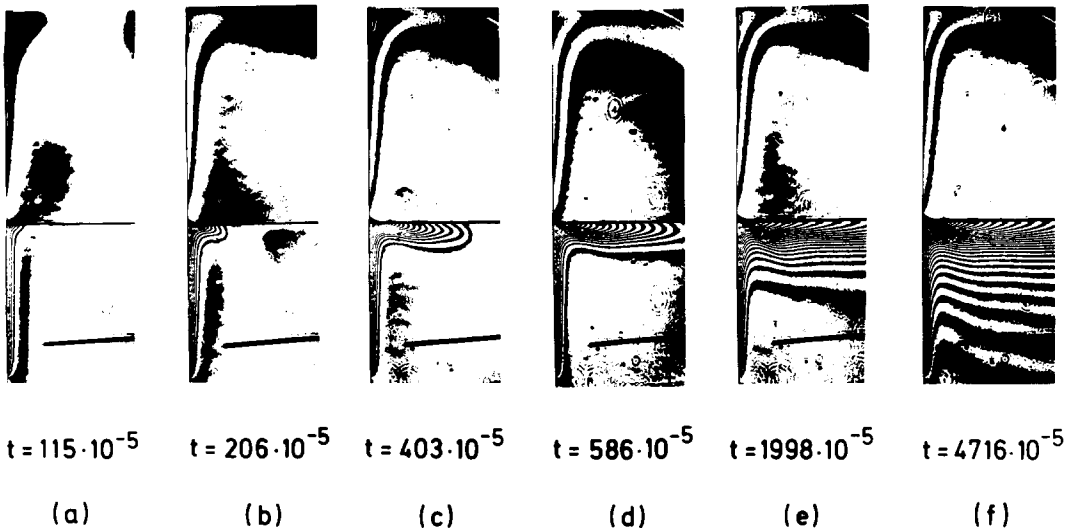

FIG. 4. Interferograms of the transient temperature field about the heated vertical plate partially immersed in water ($q'' = 760$ W m^{-2}, $Ra^{*-} = 1.83 \times 10^7$, $Pr^- = 6.3$, $l/L = 0.48$).

Furthermore, the rotary motion causes propagation of the isotherms towards the bottom especially in the region of the strongest back current. Reaching steady state, flow pattern and temperature field show a structure which is typical for laminar boundary-layer regimes. This regime is characterized by (1) steep gradients of the dependent variables near the plate and the bounding walls and (2) a nearly motionless core region where conduction is the dominating heat transport mechanism leading to the stable thermal stratification shown in Fig. 3(f).

A comparable sequence of interferograms which confirm the numerical predictions is given in Fig. 4. As the refractive indices of air and water differ, strongly quantitative interferograms could be obtained for the water layer only. Nevertheless the timewise development of the transient process is visualized clearly. The isotherms near the interface, however, have different shapes during the transient inasmuch as the interference fringes are bent backward. This may be possibly due to three-dimensional effects leading to locally different optical distances or to the kinematic behavior of the interface. It is well known (e.g. [22]) that contamination of an interface by a few layers of molecules is sufficient to make the interface as 'stiff' as a diaphragm. As mentioned above, Stork [2] found an analogous behavior by experimental observations of two superposed liquids. In order to substantiate this hypothesis a numerical calculation with the kinematic no-slip condition ($w^i = 0$) at the interface for the same set of parameters was performed. The results are depicted in Fig. 5. Comparing plots and experimental findings the similar structure of the temperature fields near the interface is evident. While the formation of the streamlines in the liquid differs from that in Fig. 3, flow pattern and temperature fields in the upper half of the container remain nearly unchanged. Although the assumption of the no-slip condition leads to altered transient temperature fields in the water layer, the calculated surface temperatures are identical in both cases.

After qualitative description of the transient

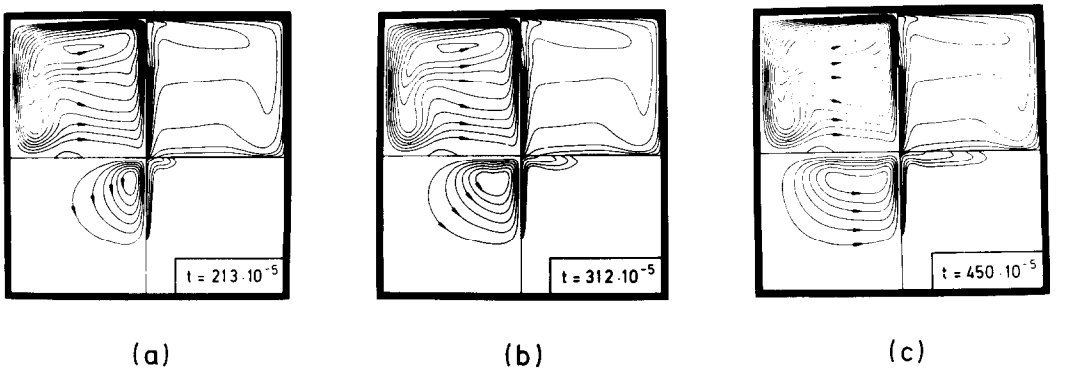

FIG. 5. Streamlines and temperature distribution at different dimensionless times for the assumption of no slip condition at the interface ($Ra^{*-} = 2.8 \times 10^7$, $l/L = 0.5$, $Pr^+ = 0.7$, $Pr^- = 7.0$).

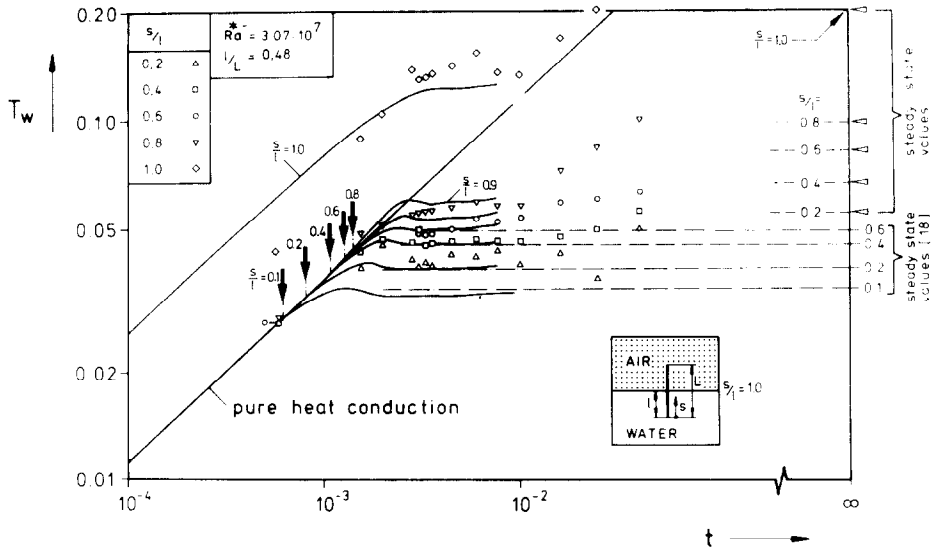

FIG. 6. Transient surface temperatures for that part of the plate exposed to water. The numerical solution is based on $Ra^{*-} = 2.8 \times 10^7$, $Pr^- = 7.0$ and $l/L = 0.5$. Experimental data are represented by symbols.

response, attention will now be focused upon quantitative heat transfer results. Because the heat flux is prescribed at the surface of the plate, the calculation of the unknown temperatures is the intrinsic problem. Using the temperature of the bounding walls for reference, the resulting dimensionless surface temperatures $T_w = (T - T_0)k^-/(q''L_0)$ may be related to the Nusselt number by

$$Nu = 1/T_w. \tag{19}$$

A representative transient surface temperature history for that portion of the plate immersed in water is shown in Fig. 6. As mentioned above, heat transfer is due to heat conduction during the early stages of the transient process. For short times such processes are always one-dimensional, even if a leading edge does exist. The analytical solution of the one-dimensional heat conduction equation

$$T_w = 2(t/\pi)^{1/2} \tag{20}$$

therefore is plotted in Fig. 6 for comparison. Numerical and experimental results show, that this assumption is valid over a limited time interval for positions $s/l < 0.8$. Due to the high temperature level in the air layer, surface temperatures above $s/l = 0.8$ deviate considerably. During the one-dimensional process the only velocity component is the one parallel to the surface. Thus, a one-dimensional layer of fluid near the surface moves upwards and grows with time. As the flow field develops an entrainment velocity this process ends in what is known as the 'leading edge effect', first pointed out by Goldstein and Briggs [23] and confirmed by Gebhart and co-workers [24–26] experimentally and numerically. Excluding other heat transport mechanisms than one-dimensional heat conduction the conservation equations simplify and may be solved analytically applying Laplace transformation. The maximum penetration depth of the leading edge effect, $y_{p\,max}$, is then calculated from the resulting velocity profile $v(x, t)$ by applying the estimation presented in [23]:

$$y_{p\,max} = \text{max. value of} \int_0^t v(x, t)\,dt. \tag{21}$$

This distance is then used to calculate the length of time after initiation of the transient in which pure conduction solution might be expected to apply locally at $y_{p\,max}$, i.e. before true convection effects are felt. The time intervals predicted in this way, however, are longer than those observed [24, 25]. As pointed out in [23] a possible reason for the discrepancy could be neglecting the convective and pressure effects across the leading edge disturbance wave in the analysis. Extensive measurements performed by Mahajan and Gebhart [25] show that the real period is about 2/3 of the theoretical prediction. Taking into account this fact, the analysis yields the following relation between nondimensional distance $s/l (\equiv y_{p\,max})$ and time:

$$t = 0.667\,[(s/l)/\zeta Ra^{*-}]^{2/5}. \tag{22}$$

The value of ζ depends upon the Prandtl number and is found by analysis to be 0.13 for $Pr^- = 7.0$. The corresponding dimensionless times calculated by expression (22) for various distances s/l are marked by bold arrows in Fig. 6. The agreement between theoretical prediction and numerical as well as experimental findings, i.e. branching off from the conduction solution, is found to be very good.

The transition period, which follows the conduction phase, may be clearly divided into three distinct parts. First, the surface temperature traces branch off of the conduction solution and pass a local maximum which is characteristic for plates with negligible heat capacity

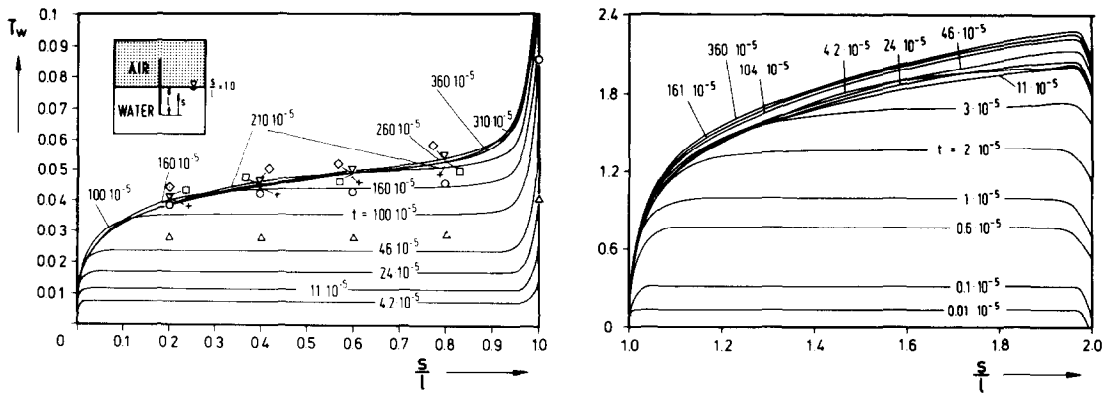

FIG. 7. Dimensionless temperature along the surface of the plate as a function of dimensionless time: (a) water, (b) air. Numerical results for $Ra^{*-} = 2.8 \times 10^7$, $Pr^- = 7.0$, $Pr^+ = 0.7$, $l/L = 0.5$. Experimental results for $Ra^{*-} = 3.07 \times 10^7$, $Pr^- = 6.4$, $l/L = 0.48$ and dimensionless times: △, 61.3×10^{-5}; ○, 156×10^{-5}; ▽, 201×10^{-5}; □, 287×10^{-5}; ◇, 309×10^{-5}; +, 364×10^{-5}.

[26, 27]. Then the temperatures decrease to a value which remains nearly constant over a limited time interval. During this period calculated as well as measured temperatures for $s/l < 0.7$ agree quite well with those found by Sparrow and Gregg [18] for a plate located in an infinite surrounding. After this phase temperatures increase again and reach the steady state asymptotically. Due to different flow conditions in the vicinity of the interface the surface temperature traces for $s/l > 0.8$ differ from those described above. For $s/l = 1$ the temperature branches off from the conduction solution shortly after loading the surface with a constant heat flux. In contrast to positions $s/l < 0.8$ the surface temperature exceeds that resulting from (20), increases rapidly, passes only a slight maximum and reaches the steady-state value subsequently.

Figure 7 shows the calculated transient surface temperature profiles along the plate for both fluid regions together with comparable experimental data. Excepting the vicinity of the interface and of the leading and trailing edge the temperature values remain constant along the depth of immersion for a limited time period, indicating the heat conduction is the dominating heat transfer mechanism. This one-dimensional conduction process at any downstream location lasts until the leading-edge effect reaches that position and convection sets in. This effect may be realized in both fluids by the departure from the constant value trace. Proceeding with time, this disturbance propagates from the leading edge (water) and interface (air) in direction to the interface and trailing edge, respectively. Considering that part of the plate exposed to air, Fig. 7(b) reveals that the temperature rises with increasing s/l and drops sharply after reaching the maximum close to the trailing edge. The temperature drop is due to the fluid motion directed towards the surface which enhances heat transfer near the upper end of the plate. Furthermore, transient response is much faster and the temperatures are much higher than in the liquid phase.

6.2. *Steady-state heat transfer*

Stream function and temperature distributions for $Ra^{*-} = 10^4$ and 10^7 and for various depths of immersion l/L are presented in Fig. 8 for steady-state heat transfer condition. Attention is first focused upon the water layer. Isotherms and streamlines for $Ra^{*-} = 10^4$ indicate that there is only a small effect of the depth of immersion, which will be further reduced for increasing Rayleigh number. Due to the distributions of the fields of variables the heat transfer characteristics may be related to transition and laminar boundary-layer regime for $Ra^* = 10^4$ and 10^7, respectively. Considering the corresponding contour maps for the gas region, different regimes are detectable. While the heat transfer modes for the case $l/L = 0.25$ and $Ra^{*-} = 10^4$ may also be related to the transition regime an increasing depth of immersion leads to a distribution of the variables which are typical for conduction regimes. This behavior may be explained by the Rayleigh number Ra^{*+} characterizing heat transfer in the upper part of the container. Both Rayleigh numbers are linked by

$$Ra^{*+} = (\phi_3/\phi_2\phi_4\phi_6)(L/l-1)^4\, Ra^{*-} = \tilde{\phi}\, Ra^{*-}. \quad (23)$$

Using the relations given in (18) the following multiplication factors $\tilde{\phi}$ result:

l/L	0.25	0.50	0.75
$\tilde{\phi}$	13.6	0.168	2.07×10^{-3}.

The determined steady-state temperature profiles along the surface of the plate are reproduced in Fig. 9 for $l/L = 0.5$ and various Rayleigh numbers together with experimental data. All curves show that the dimensionless temperature niveau decreases with increasing Rayleigh number. One has to bear in mind, however, that for constant l/L the heat flux density has

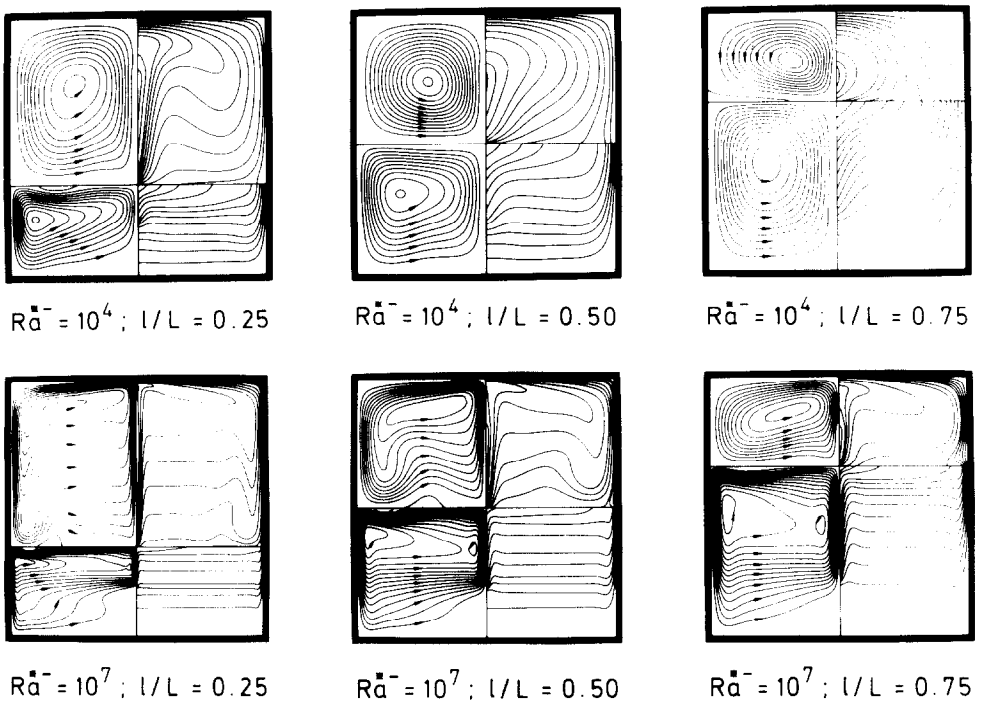

FIG. 8. Numerical contour maps of isotherms (right) and stream function (left) for various Rayleigh numbers and depths of immersion ($Pr^- = 7.0$, $Pr^+ = 0.7$).

to be enhanced to get higher Rayleigh numbers and therefore the real temperatures increase too. The surface temperature on that portion of the plate immersed in water is minimum at the leading edge, because there is the smallest thickness of the boundary layer. As expected, the maximum temperature is found at the interface. It is seen from Fig. 9(a), that all profiles flatten with increasing Rayleigh number, due to enhanced convective motion. Except for the regions next to the leading edge and the interface this results in nearly linear temperature distributions. A similar trend may be found for the temperature profiles along that part of the plate exposed to air. As mentioned above the minimum temperature occurs at the interface whereas the maximum is reached a short distance downstream of the trailing edge. This maximum travels in this direction to the upper edge of the plate and levels off with increasing Rayleigh number. Due to the thermophysical properties of air the plate is heated to much higher temperatures than that portion of the plate exposed to water. For $Ra^{*-} = 10^7$ the maximum surface temperature in air is about 12 times higher than that in water. For the sake of clearness presentation was restricted to one depth of immersion. It should be

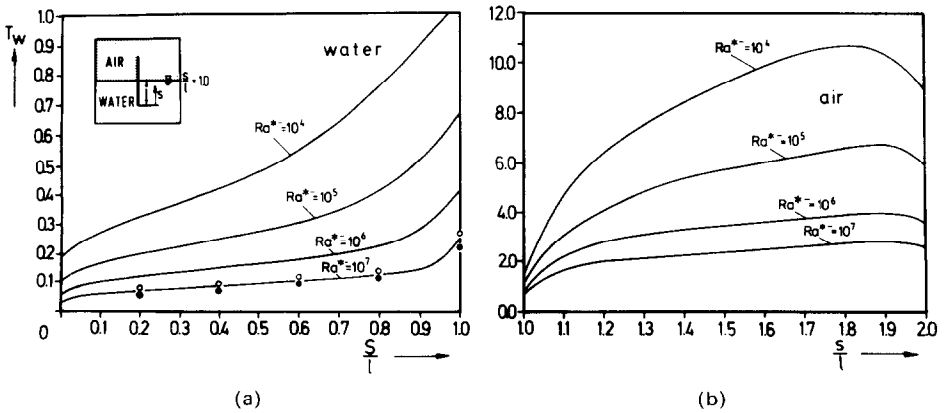

FIG. 9. Steady-state temperature profiles along the surface of the vertical plate for various Rayleigh numbers and $l/L = 0.5$ ($Pr^- = 7.0$, $Pr^+ = 0.7$). Experimental data: ○, $l/L = 0.47$, $Ra^{*-} = 1.6 \times 10^7$; ●, $l/L = 0.43$, $Ra^{*-} = 2.06 \times 10^7$.

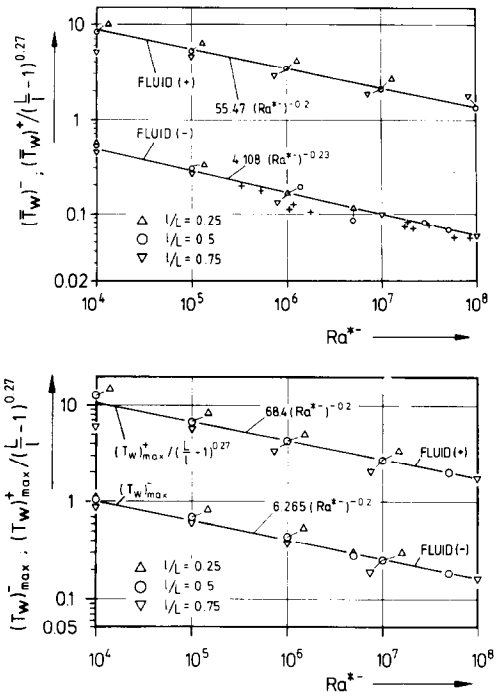

FIG. 10. Average and maximum dimensionless surface temperatures $\bar{T}_w$ and $T_{w\,max}$ for various depths of immersion as function of the Rayleigh number Ra^{*-}.

noted, however, that the temperature profiles for $l/L = 0.25$ and 0.75 are nearly identical for $Ra^{*-} > 10^6$, indicating that the temperature distribution is only influenced for small Rayleigh numbers which was already expected from the contour plots shown in Fig. 8. Using a regression analysis calculated and measured maximum and average surface temperatures may be correlated by the following equation:

$$(\bar{T}_w; T_{w\,max}) = \varepsilon_1 (L/l - 1)^{\varepsilon_2} (Ra^{*-})^{\varepsilon_3} \qquad (24)$$

		ε_1	ε_2	ε_3
air	$\bar{T}_w$	55.47	0.27	−0.2
	$T_{w\,max}$	68.40	0.27	−0.2
water	$\bar{T}_w$	4.108	0.0	−0.23
	$T_{w\,max}$	6.265	0.0	−0.2

All correlations are presented graphically in Fig. 10 as a function of the Rayleigh number Ra^{*-}. Comparing equation (24) with the data obtained by numerical analysis and by experiment good agreement is found, except for small Rayleigh numbers. This is due to the additional geometric dependence already mentioned.

7. CONCLUDING REMARKS

The characteristics of transient and steady-state heat transfer from a vertical flat plate loaded by a constant heat flux and partially immersed in water is studied theoretically and by experiment. The analytical results were obtained by numerical solution of the complete set of conservation equations based on the primitive variables. The discretized equations were solved by a fully implicit procedure. The Poisson–Neumann problem associated with the calculation of pressure is solved efficiently by means of a multi grid method.

Experimental as well as numerical results of the problem studied should be summarized as follows:

- During the early stages after loading the plate with a constant heat flux heat is transferred solely by conduction.
- The transient response depends on the thermophysical properties of the wetting fluid. It is shorter for that part of the plate exposed to air than that exposed to water.
- Surface temperatures and duration of the one-dimensional transient may be described analytically for those positions of the plate far enough downstream of the interface. After passing local maxima the surface temperatures rise again, reaching the steady-state values asymptotically.
- Average and maximum steady-state values are satisfactorily expressed by correlation equations.

Owing to the general formulation the developed code is applicable to many classes of conceivable configurations without additional effort. Further studies are therefore directed to problems involving the influence of different thermophysical properties as well as thermocapillary convection on natural convection heat transfer in arbitrarily shaped geometries.

Acknowledgement—The authors wish to express their appreciation for the support of this work by the Deutsche Forschungsgemeinschaft—DFG.

REFERENCES

1. J. Szekely and M. R. Todd, Natural convection in a rectangular cavity transient behavior and two phase systems in laminar flow, *Int. J. Heat Mass Transfer* **14**, 467–482 (1971).
2. K. W. Stork, Zellularkonvektion in Behältern und in geschichteten Flüssigkeiten. Doctoral thesis, Universität Karlsruhe (1974).
3. R. Schramm and H. H. Reineke, Natural convection in a horizontal layer of two different fluids with internal heat sources, *Proc. 6th Int. Heat Transfer Conference*, Vol. 2, pp. 299–304 (1978).
4. G. I. Bourde and I. B. Simanovskii, Determination of equilibrium boundaries of a two-layer sytem convection stability, *J. appl. Math. Mech.* **43**, 1091–1097 (1979).
5. I. B. Simanovskii, Numerical investigation of convection in a system of two immiscible fluids heated from below. In *Convection Flows and Hydrodynamik Stability*, pp. 126–31. Izd. Ural. Nauch. Tsentr, Akad. Nauk SSSR, Sverdlovsk (1979).
6. R. W. Knight and M. E. Palmer III, Similation of free convection in multiple fluid layers in an enclosure by finite differences. In *Numerical Properties and Methodologies in Heat Transfer* (edited by T. M. Shih), pp. 305–319. Hemisphere, Washington (1983).
7. J. F. Thompson, F. C. Thames and C. W. Mastin, Automatic numerical generation of body-fitted curvi-

linear coordinate system for field containing any number of arbitrary two-dimensional bodies, *J. comput. Phys.* **15**, 299–319 (1974).
8. U. Projahn, H. Rieger and H. Beer, Heat conduction in anisotropic composites of arbitrary shape (a numerical analysis), *Wärme-u. Stoffübertr.* **15**, 223–232 (1981).
9. U. Projahn, H. Rieger and H. Beer, A numerical analysis of laminar natural convection between concentric and eccentric cylinders, *Num. Heat Transfer* **4**, 131–146 (1981).
10. H. Rieger, U. Projahn and H. Beer, Analysis of the heat transport mechanisms during melting around a horizontal circular cylinder, *Int. J. Heat Mass Transfer* **25**, 137–147 (1982).
11. C. Truesdell and R. Toupin, The classical field theories. In *Handbuch der Physik* (edited by S. Flügge), Vol. III/1, pp. 226–793. Springer-Verlag, Berlin (1960).
12. W. Flügge, *Tensor Analysis and Continuum Mechanics*. Springer-Verlag, Berlin (1972).
13. U. Projahn, Numerische und experimentelle Untersuchung von stationären und instationären konvektiven Wärmetransportvorgängen in ein- und zweiphasigen Fluidsystemen. Doctoral thesis, Technische Hochschule Darmstadt (1984).
14. F. H. Harlow and J. E. Welch, Numerical calculation of time-dependent viscous incompressible flow of fluid with free surface, *Phys. Fluids* **8**, 2182–2189 (1965).
15. H. L. Stone, Iterative solution of implicit approximations of partial differential equations, *SIAM J. num. Analysis* **5**, 530–558 (1968).
16. H. Rieger, U. Projahn and H. Beer, Fast iterative solution of Poisson equation with Neumann boundary conditions in nonorthogonal curvilinear coordinate systems by a multiple grid method, *Num. Heat Transfer* **6**, 1–15 (1983).
17. W. Hauf and U. Grigull, Optical methods in heat transfer. In *Advances in Heat Transfer*, Vol. 6, pp. 134–366. Academic Press, New York (1970).
18. E. M. Sparrow and J. L. Gregg, Laminar free convection from a vertical plate with uniform surface heat flux, *Trans. Am. Soc. mech. Engrs* **78**, 435–440 (1956).
19. S. P. Pope, The calculation of turbulent recirculating flows in general orthogonal coordinates, *J. comput. Phys.* **26**, 197–217 (1978).
20. C. R. Illingworth, Unsteady laminar flow of a gas near an infinite plate, *Proc. Camb. phil. Soc.* **46**, 603–613 (1950).
21. B. Sammakia, B. Gebhart and Z. H. Qureshi, Measurements and calculations of transient natural convection in water, *J. Heat Transfer* **104**, 644–648 (1982).
22. K. L. Wolf, *Physik und Chemie der Grenzflächen*, Vols. 1 and 2. Springer-Verlag, Berlin (1957, 1959).
23. R. J. Goldstein and D. G. Briggs, Transient free convection about vertical plates and cylinders, *J. Heat Transfer* **86**, 490–500 (1964).
24. B. Gebhart and R. P. Dring, The leading edge effect in transient natural convection from a vertical plate, *J. Heat Transfer* **89**, 274–275 (1967).
25. R. L. Mahajan and B. Gebhart, Leading edge effects in transient natural convection flow adjacent to a vertical surface, *J. Heat Transfer* **100**, 731–733 (1978).
26. B. Sammakia and B. Gebhart, Transient and steady-state numerical solutions in natural convection, *Num. Heat Transfer* **1**, 529–542 (1978).
27. B. Sammakia and B. Gebhart, Transient natural convection adjacent to a vertical flat surface: the thermal capacity effect, *Num. Heat Transfer* **4**, 331–344 (1981).

ETUDE THEORIQUE ET EXPERIMENTALE DU TRANSFERT DE CHALEUR STATIONNAIRE ET INSTATIONNAIRE D'UNE PLAQUE PLANE VERTICALE EN PARTIE IMMERGEE

Résumé—Le comportement stationnaire et instationnaire du transfert thermique d'une plaque plane verticale dû à la convection naturelle est étudié numériquement et expérimentalement. La plaque, qui se trouvre dans un récipient cubique rempli en partie d'un liquide, en partie d'un gaz, libère un flux de chaleur uniforme et constant. Les calculs numériques donnent des solutions pour une série de différents rapports de propriétés physiques et pour des nombres modifiés de Rayleigh allant jusqu'à $Ra^{*-} = 10^8$, ce qui est aussi pris en compte dans les expériences. Une comparaison entre résultats calculés et expérimentaux montre un bon accord.

THEORETISCHE UND EXPERIMENTELLE UNTERSUCHUNG DES STATIONÄREN UND INSTATIONÄREN WÄRMETRANSPORTS VON EINER VERTIKALEN, TEILWEISE IN WASSER EINGETAUCHTEN EBENEN PLATTE

Zusammenfassung—Das stationäre und instationäre Wärmeübertragungsverhalten infolge natürlicher Konvektion an einer vertikalen ebenen Platte wurde numerisch und experimentell untersucht. Die mit einem gleichförmigen und konstanten Wärmestrom beaufschlagte Platte befindet sich in einem quadratischen Behälter, der teilweise mit Flüssigkeit und Gas gefüllt ist. Die numerischen Berechnungen umfassen Lösungen für einen Satz von Stoffwertverhältnissen und für modifizierte Rayleighzahlen bis $Ra^{*-} = 10^8$, was ebenfalls durch die Experimente überdeckt wird. Ein Vergleich zwischen gerechneten und gemessenen Ergebnissen zeigt eine gute Übereinstimmung.

ТЕОРЕТИЧЕСКОЕ И ЭКСПЕРИМЕНТАЛЬНОЕ ИЗУЧЕНИЕ ПЕРЕХОДНОГО И СТАЦИОНАРНОГО РЕЖИМОВ ЕСТЕСТВЕННОКОНВЕКТИВНОГО ТЕПЛОПЕРЕНОСА ОТ ВЕРТИКАЛЬНОЙ ПЛОСКОЙ ПЛАСТИНЫ, ЧАСТИЧНО ПОГРУЖЕННОЙ В ВОДУ

Аннотация—Проведено численное и экспериментальное изучение переходного и стационарного естественноконвективного теплопереноса от вертикальной плоской пластины. Пластина, нагреваемая однородным постоянным тепловым потоком, помещалась в квадратную емкость, частично заполненную жидкостью и газом. Решения получены для одного набора значений теплофизических свойств и для модифицированных чисел Рэлея вплоть до $Ra^{*-} = 10^8$. В этом же диапазоне проведены и эксперименты. Получено хорошее соответствие между результатами расчетов и измерений.